Available online at www.sciencedirect.com
SCIENCE DIRECT
Journal of Molecular Catalysis A: Chemical 240 (2005) 214–225
JOURNAL OF MOLECULAR CATALYSIS A: CHEMICAL
www.elsevier.com/locate/molcata

Impact of the urea–matrix combustion method on the HDS performance of Ni-MoS_2/γ-Al_2O_3 catalysts

Sergio L. González-Cortés *, Tian-Cun Xiao, Serbia M.A. Rodulfo-Baechler, Malcolm L.H. Green

Wolfson Catalysis Centre, Inorganic Chemistry Laboratory, University of Oxford, South Parks Road, Oxford OX1 3QR, UK

Received 12 May 2005; received in revised form 8 June 2005; accepted 8 June 2005
Available online 8 August 2005

Abstract

A detailed study has been made of the different steps involved upon the preparation of γ-Al_2O_3-supported Ni-Mo HDS catalyst precursors by urea–matrix combustion (UMxC) method. Catalyst performance was evaluated using a tubular fixed-bed reactor and the hydrodesulfurization of thiophene under normal pressure as a model reaction. The oxidic and sulfurized states of the HDS catalysts were characterized by X-ray diffraction (XRD), laser Raman spectroscopy, thermogravimetric analysis (TGA), differential scanning calorimetry (DSC) and high resolution transmission electron microscopy (HRTEM) in order to correlate their oxidic and sulfurized properties with the catalytic behaviour. During the UMxC process several consecutive stages such as melting, dissolution and chemical reactions occurred. There was no evidence of residual carbon and well-dispersed Ni- and Mo-oxo-species supported on alumina were formed.

Urea employed as fuel not only increases the combustion rate, but also undergoes a decomposition process (endothermic reaction) that could contribute to the reduction of the combustion temperature. The urea–matrix combustion method permit to synthesize highly active γ-Al_2O_3-supported Ni-Mo HDS catalysts with a comparable promoter effect than that of corresponding catalyst prepared by impregnation method. In addition, an opposite relation between the activity and the hydrogenation properties was observed indicating that highly active HDS catalyst requires low consumption of hydrogen. Finally, both the ignition temperature and the urea-oxidizer ratio produce no significant changes in the HDS catalytic properties of Ni-Mo-based catalysts.

Keywords: Urea; HDS reactions; Ni-promoted MoS_2 catalysts; Urea–matrix combustion method

1. Introduction

The stringent environmental regulations in the US and Europe are requiring significant improvement in the quality of transportation fuel. It is directed towards reducing the amount of sulfur content in gasoline and diesel fuel to 10 ppm by 2009 [1]. Many approaches based on novel processes such as adsorption and selective oxidative desulfurization have been proposed to remove sulfur-containing compounds from petroleum feedstocks to meet this requirement [2], whereas others are based on the improvement of current hydrotreating technology. Nowadays, alumina-supported molybdenum sulphide catalysts, promoted with cobalt or nickel, are the commonly employed catalysts for HDS reactions of fossil fuels due to their high activity and stability [3–7]. Supported nickel-molybdenum catalysts are usually prepared by depositing molybdenum and nickel oxides on the surface of γ-alumina (Al_2O_3). The catalysts are used in the active sulfide state and the nature and properties of the oxidic precursors largely determine the performance of the catalysts. Several studies focused on the promoter effect of Co and Ni on the oxo-Mo species indicates that both elements do not affect greatly the state of the Mo species over the γ-Al_2O_3 [8,9]. However, other studies report that the inter-

* Corresponding author. Permanent address: Laboratorio de Cinética y Catálisis, Universidad de Los Andes, Mérida 5101, Venezuela.
Tel.: +44 1865 272660; fax: +44 1865 272690.
E-mail addresses: sergio.gonzalezcortes@chem.ox.ac.uk, goncor@ula.ve (S.L. González-Cortés).

1381-1169/$ – see front matter © 2005 Elsevier B.V. All rights reserved.
doi:10.1016/j.molcata.2005.06.055

action between the oxidic precursors after the calcination process might favour either the formation of $NiMoO_4$-type phase [10] or the Ni-Mo-O species [11], which could be optima precursors for the formation of the Ni-Mo-S active phases.

We recently developed a new approach called urea–matrix combustion (UMxC) method to prepare highly active Co-promoted alumina-supported MoS_2 HDS catalysts [12]. This method, based on a self-propagating combustion reaction [13], requires low ignition temperature to induce a combustion reaction between the catalyst precursor salts and an organic matrix as the fuel. The final products of combustion might contain a high concentration of structural defects, which are beneficial as active centres in catalysis [14]. The main characteristics are complete or partial elimination of an external energy supply and very high rates of heating and cooling, while control of process rate, temperature, degree of conversion, composition and structure of products can be obtained by varying the rates of heat release and transfer [15,16]. This material synthesis method has been used to prepare catalysts for deep oxidation of methane [17], oxidative coupling of methane [18], oxidation of carbon monoxide and reduction of NO [19,20] and more recently Co-Mo HDS catalysts [12]. Since combustion synthesis is based on the transformation of the precursor salts through an exothermic reaction; it generates very high heating and cooling rates in very short period, which can lead to the formation of new highly defective structures of nanoscale meta-stable phases. This fact is particularly important for the synthesis of promoted catalysts such as HDS catalysts where the interaction between the oxidic precursors is directly related to the catalytic performance of hydrotreating catalysts [21].

In order to find out whether urea–matrix combustion method is also suitable to prepare alumina-supported Ni-promoted MoS_2 HDS catalysts, we have synthesized and studied the HDS activity of a series of catalysts with variable Ni loadings. The molybdenum oxide content was maintained constant at 12 wt.%. In addition, we have carried out a detailed thermo-chemical examination of the urea–matrix combustion method in order to determine the influence of molybdenum precursor (i.e., ammonium heptamolybdate) and the fuel-oxidizer ratio on the combustion process.

2. Experimental

2.1. Preparation of the oxidic precursors

Bimetallic Ni-Mo catalyst precursors with 12 wt.% MoO_3 and variable NiO composition supported on γ-Al_2O_3 (164 m^2/g) were prepared by mixing urea with ammonium heptamolybdate-4-hydrate and Ni(II) nitrate employing variable urea/(Mo + Ni) molar ratio and ca. 1 g/2 mL = (Ni- and Mo-precursors + urea)/water ratio. This mixture was stirred to form a homogeneous slurry, then mixed with the γ-Al_2O_3 support at ca. 50 °C for 2–3 h to obtain urea-based slurry containing nickel and molybdenum fully loaded over the alumina. The resulting paste was divided in two portions: (i) a part was dried under high vacuum (ca. 10^{-4} Torr) for 24 h in order to study the combustion process using TGA–DSC and (ii) another part is ignited at 500 °C (furnace temperature) in static air for 10 min to produce a yellow oxide catalyst precursor material.

2.2. Sulfurization and catalytic tests

The HDS reactions free of mass transport interference were carried out in a fixed-bed tubular quartz reactor (34 cm long, 4 mm i.d.). Oxidic catalyst precursors (200 mg, <250 μm) were loaded between quartz wool plugs. The activation (e.g., sulfurization) process was done using a 20 mL min^{-1} hydrogen (ultra high purity) flow rate, which passed through a thiophene (99+%, Aldrich) saturator at room temperature (10.9 kPa). All lines located after the saturator were heated at temperature high enough to avoid thiophene condensation. The furnace temperature is increased linearly from room temperature to 450 °C at 5 °C min^{-1} and held at 450 °C for 10 h. Then, the sample was treated with a pure H_2 flow at 450 °C for 1 h and cooled down to 350 °C. The catalysts were tested at atmospheric pressure (0.1 MPa) and the reactants consisted of a 20 mL min^{-1} H_2 flow saturated with thiophene vapour at 0 °C (2.96 kPa), resulting in a mixture of ca. 3 mol% thiophene in H_2. The reaction products were analyzed using an on-line HP 5890 Series II chromatograph equipped with a Hayesep R packed column and a flame ionization detector (FID). After completion of the catalytic reaction, the catalyst sample was cooled down to room temperature under flowing argon and then passivated before exposure to the atmosphere and kept in a desiccator thereupon.

2.3. Characterization of the precursors and HDS catalysts

The crystalline phases of the oxidic precursors and the sulfurized catalysts were identified by X-ray diffraction (XRD) in a Philips PW1710 diffractometer equipped with an X-ray tube (Cu Kα radiation λ = 1.5406 Å; 40 kV, 30 mA). The specimen were prepared by grinding a small amount of each sample using an agate mortar and pestle and then loaded into a flat sample holder. The data were collected in $\theta/2\theta$ reflection mode, from 3 to 70° in 2θ, using steps of 0.05°, with time per step of 1.25 s.

Thermogravimetric analysis (TGA) and differential scanning calorimetry (DSC) were simultaneously carried out on a Rheometric Scientific STA 1500 instrument. TGA–DSC profiles were recorded from room temperature to 750 °C, using 30 mL min^{-1} dry air flow and 10 °C min^{-1} heating rate. For each analysis ca. 25–35 mg of sample was loaded into a small alumina crucible, using alumina as reference.

The Raman spectra of the oxidic precursors and the sulfurized catalysts were recorded in an Yvon Jobin Labram spectrometer with a 632 nm HeNe laser, run in a back-scattered co-focal arrangement. The samples were pressed in a microscope slide; with a 45 s scanning time and 2 cm^{-1} resolution. Several points of each catalyst surface were probed to explore homogeneity of the sample and reproducibility of the data.

High resolution transmission electron microscopy (HRTEM) was carried out using a JEOL 4000FX electron microscope with a 400 kV accelerating voltage. Ni-Mo sulfurized catalyst was ground into a fine powder and dispersed in AR-grade chloroform. Then, it was placed in an ultrasonic bath for ca. 15 min, before a drop of the suspension was put on a lacey carbon-coated copper grid (Agar, 20 mesh) and subsequently analyzed.

3. Results and discussion

3.1. Study of the combustion–decomposition processes of the urea–matrix prepared catalysts

The TG curves and the differential TG profiles (inset) of the urea-containing Ni-Mo precursor salts are given in Fig. 1A. The major weight loss (WL) for the monometallic (i.e., Ni and Mo) and bimetallic (Ni-Mo) precursor thermograms takes place in the 130–300 °C range and it is attributed to a complex series of overlapping chemical reactions such as the partial dehydroxylation of alumina [22] and the partial dehydration and decomposition of the hydrated nickel nitrate and ammonium heptamolybdate salts [23–26]. In addition, weight losses at temperatures greater than 300 °C for the monometallic oxidic precursors are observed (Fig. 1Aa and

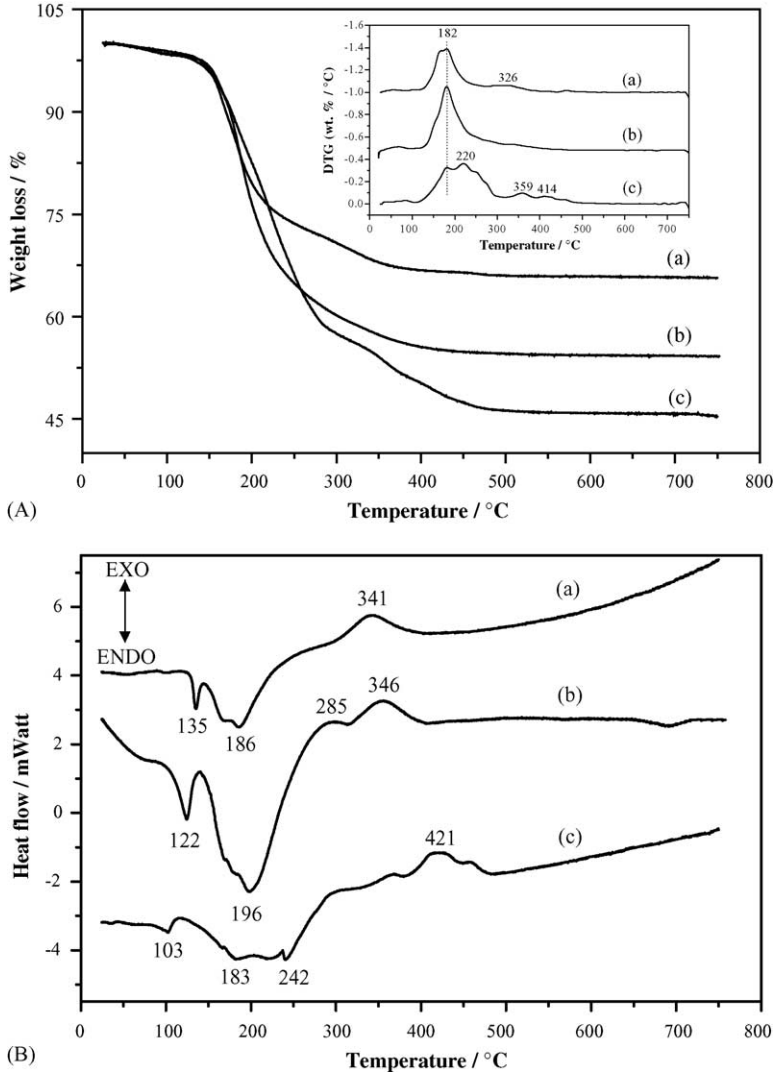

Fig. 1. (A) Thermogravimetric profiles of the γ-alumina-supported Ni-Mo precursor salts with urea/metals mole ratio of 10 and dried at room temperature in high vacuum (∼10^{-4} Torr). Inset is the differential TG profiles. (a) 12 wt.% MoO_3/γ-Al_2O_3, (b) 3 wt.% NiO-12 wt.% MoO_3/γ-Al_2O_3, (c) 12 wt.% NiO/γ-Al_2O_3. (B) Differential scanning calorimetry curves of the γ-alumina-supported Ni-Mo precursor salts with urea/metals mole ratio of 10 and dried at room temperature in high vacuum. (a) 12 wt.% MoO_3/γ-Al_2O_3, (b) 3 wt.% NiO-12 wt.% MoO_3/γ-Al_2O_3, (c) 12 wt.% NiO/γ-Al_2O_3.

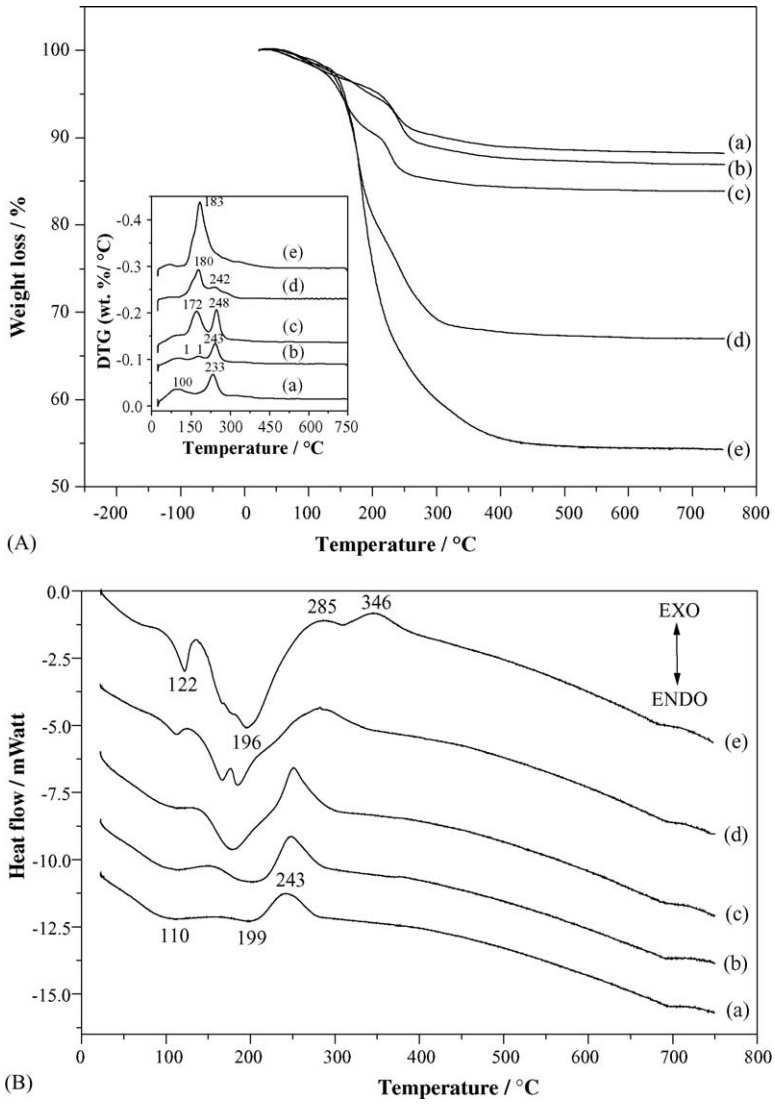

Fig. 2. (A) Thermogravimetric profiles of the γ-alumina-supported Ni-Mo precursor salts (i.e. 3 wt.% NiO-12 wt.% MoO_3) containing different urea/(Ni + Mo) mole ratio and dried at room temperature in high vacuum. Inset is the differential TG profiles. (a) 0.0, (b) 0.25, (c) 1.0, (d) 5.0, (e) 10.0. (B) Differential scanning calorimetry of the γ-alumina-supported Ni-Mo precursor salts (i.e. 3 wt.% NiO-12 wt.% MoO_3) containing different urea/(Ni + Mo) mole ratio and dried at room temperature in high vacuum. (a) 0.0, (b) 0.25, (c) 1.0, (d) 5.0, (e) 10.0.

Ac). The total weight losses coincided with the expected values (assuming the formation of nickel and molybdenum oxides), indicating that both the urea and the precursor salts are completely decomposed without residue of carbon.

The DSC profiles of the urea-containing Ni-Mo precursor salts are given in Fig. 1B. It shows several endothermic processes at temperatures lower than 250 °C and different exothermic reactions at higher temperatures. A narrow endothermic peak at 135 °C associated with the melting process of urea is shown in the DSC curve of 12 wt.% MoO_3/γ-Al_2O_3 oxidic precursor (see Fig. 1Ba) [25]. A similar stage is also observed in the profiles of Ni-Mo and Ni precursors (see Fig. 1Bb and 1Bc), however the peak position is clearly shifted to lower temperature and becomes broader with increasing of NiO loading. This trend can be due to the presence of an urea ↔ nickel nitrate interaction and/or the depressed effect of impurities on the melting point of urea (i.e. colligative property).

On the other hand, a broad endothermic band occurs in the same temperature range that the major weight loss takes place and subsequently the sample underwent the combustion process. This sequence of processes suggests that the thermal decomposition of urea might play a very important role as an attenuating process of the maximum combustion temperature. These processes (i.e., decomposition and combustion) can be overlapped as occurred in the Ni-Mo oxidic precursor or can take place at temperature clearly different as occurred in the monometallic precursors. On the other hand, not only the peak position of the heat flow liberated during combustion reaction, but also the enthalpy of the combustion processes depends markedly on the catalyst composition.

The TG and differential TG profiles (inset) of the urea-containing alumina-supported Ni-Mo precursor salts, corresponding to 3 wt.% NiO-12 wt.% MoO_3/γ-Al_2O_3 oxidic precursor, are given in Fig. 2A. The sample free of urea presents two major weight losses of 3.5 and 7.8 wt.% maximized at ca. 100 and 233 °C, respectively (Fig. 2Aa). The former is due to the desorption of physically adsorbed water on alumina surface [27,28] and the latter is attributed to a complex series of overlapping chemical reactions, such as the partial dehydroxylation of alumina [22] and the partial dehydration-decomposition and the subsequent total transformation of the Ni and Mo precursor salts into the catalyst oxidic precursor [23–26]. The presence of urea (i.e., urea/(Ni + Mo) of 0.25) produces a new weight loss step maximized at intermediate temperature (i.e., 181 °C) (Fig. 2Ab) this step becomes greater and asymmetric with the increase of urea content. Simultaneously, the weight loss step at higher temperature undergoes both a slight increase of the maximum temperature and a clear descent of its intensity compared with the stage at intermediate temperature. This effect is notable for the precursor containing an urea/(Ni + Mo) ratio of 10 where one major weight loss at 183 °C is observed see (Fig. 2Ae).

The DSC profiles of the alumina-supported Ni-Mo precursor salts are shown in Fig. 2B. DSC curve of the urea-free sample displays two broad endothermic processes centred at ca. 110 and 199 °C and one narrow exothermic at 243 °C (Fig. 2Ba). The first stage is mainly due to water desorption and the second one is associated with the partial dehydration-decomposition of the Ni and Mo precursor salts, whereas the third stage at 243 °C is assigned to an exothermic process that leads to total transformation of the partially decomposed Ni and Mo precursors into the catalyst oxidic precursor. The DSC profiles of the urea-containing precursors display a similar thermal behaviour to that of the urea-free sample. However, the major endothermic band becomes stronger and asymmetric, due to the decomposition of urea, leading to the formation of two well defined peaks when urea/(Ni + Mo) ratio is 5.0 and a broad band for an urea/(Ni + Mo) ratio of 10 (Fig. 2Bd and Be) is observed. Also, these profiles displayed a small endothermic peak at temperatures clearly lower than the melting point of urea (i.e., 135 °C [25]), probably due to the presence of ionic species within urea crystal structure that reduce its melting temperature (colligative property). On the other hand, the exothermic feature is slightly shifted to higher temperatures and becomes narrow whereas the urea/(Ni + Mo) ratio increased up to 1.0. A further rise of urea content leads to a widening and shift of the stage to higher temperature and also produces a second exothermic process at 346 °C when the urea/(Ni + Mo) ratio is 10 due to further combustion of residual organic matrix.

The experimental and theoretical total weight losses and combustion rates of alumina-supported 3Ni-12Mo catalyst precursors are listed in Table 1. The experimental total weigh losses are very close to the theoretical total weight losses, especially at high urea compositions. This suggests that during the combustion process the Ni and Mo oxidic precursors are not lost by volatilization and also that carbon material does not remain in the catalyst precursor. Therefore the extent of combustion reaction based on the carbon content is complete. On the other hand, the weight loss by combustion against total weight loss (i.e., $WL_{Comb}/WL_{Exp}^{Total}$) for urea-free precursor is clearly greater than those for urea-containing precursors. This finding is attributed to the notable contribution of the urea thermal decomposition over the total weight loss even at a composition close to the stoichiometric composition of the redox mixture (i.e., urea/(Ni + Mo) = 0.27). Under this optimal composition the total oxidizing and reducing valences of the oxidizer–fuel mixture is unity, according to the propellant chemistry and hence the energy released during the combustion is maximum [29–31]. Indeed, the combustion enthalpy of the urea-containing precursor (i.e., urea/(Ni + Mo) = 0.25) is ca. 32% greater than that produced by urea-free precursor, a quite similar trend is also observed for the combustion rates, Table 1. A global analysis of these results indicates that the increase of the urea loading facilitates the urea partial thermal decomposition before starting the combustion reaction at the ignition temperature of ∼200 °C and both processes are overlapped when high urea composition is employed. In consequence, the combustion temperature could be markedly lower than that of the sample prepared from the urea/(Ni + Mo) ratio of 0.25.

The combustion reactions can reach extremely high temperatures within very short time. It is therefore reasonable to assume that a thermally isolated system exists because there is very little time for the heat to disperse to its surroundings. Therefore, the maximum temperature achieved by the reaction products is assumed to be adiabatic temperature (T_{ad}),

Table 1
Weight losses and combustion rates of 3% NiO-12% MoO_3/γ-Al_2O_3 prepared by urea–matrix combustion method

Urea/(Ni + Mo) mole ratio	$WL_{Theor.}^{Total}$ (%)	$WL_{Exp.}^{Total}$ (%)	$WL_{Comb.}/WL_{Exp.}^{Total}$ (%)	Combustion rate[a] (WL%/°C) × 10^4
0.0	10.4	11.3	69.0	1009.7 ± 5.3
0.25	11.9	13.2	56.8	1389.7 ± 5.2
1.0	16.1	16.3	39.3	1463.9 ± 6.5
5.0	32.9	33.0	37.6	1429.1 ± 1.9
10.0	46.4	45.5	nd	nd

WL, weight loss; nd, value not determined because of overlapping of combustion and decomposition processes.
[a] Slope of TGA curve in the 200–250 °C region with a correlation coefficient greater than 0.999.

which can be calculated using the Eq. (1) [32]:

$$-\Delta H_r^\circ = \int_{T_0}^{T_{ad}} C_p(\text{products})\,dT \quad (1)$$

where ΔH_r° is the enthalpy of reaction at T_0 (298 K) and C_p is the heat capacity of the products at T_0. The optimal composition of urea was worked out using the total oxidizing and reducing valencies of the components, so that the equivalence ratio is unity [30]. The reducing valences of ammonium heptamolybdate and urea are +18 and +6, respectively, whereas the oxidizing valence of nickel (II) nitrate is −10, considering the corresponding valencies of the metals, −2 for oxygen and zero (0) for nitrogen.

Considering the reducing/oxidizing valencies of the starting materials and the required catalyst composition (i.e., Ni/Mo molar ratio), it is possible to determine the amount of urea necessary to obtain an optimal redox mixture. For instance, for the synthesis of $NiMoO_4$ (Ni/Mo = 1) and assuming that under stoichiometric composition urea decomposed to CO_2, H_2O and N_2 the overall reaction is:

$$21Ni(NO_3)_2{\cdot}6H_2O + 3(NH_4)_6Mo_7O_{24}{\cdot}4H_2O + 26CO(NH_2)_2 \rightarrow 21NiMoO_4 + 226H_2O + 26CO_2 + 56N_2 \quad (2)$$

Using the relevant thermodynamic data [25,33–35], we calculated the enthalpy change involved in the chemical reaction (2) and subsequently the adiabatic temperature employing the Eq. (1).

The adiabatic temperatures and the redox mixture compositions against the catalyst molar compositions are represented graphically in Fig. 3. This reveals that small increases of the Mo/Ni molar ratio produce strong rises of the adiabatic temperature until the system achieves temperatures that induce phase transitions and likely Mo-species volatilization when Mo/Ni ratio is greater than 1. This fact attenuates the increase of the adiabatic temperature. On the other hand, the urea-oxidizer mixture composition continuously decreases as the Mo/Ni mole ratio is raised. Considering this opposite behaviour it is inferred that ammonium heptamolybdate acts as fuel upon combustion process. It is supported not only by the exothermic stage displayed in the DSC profile of the urea-free precursor (see Fig. 2Ba), but also by the clear increase of the adiabatic temperature whereas Mo composition is increased despite the lower urea composition present in the redox mixture.

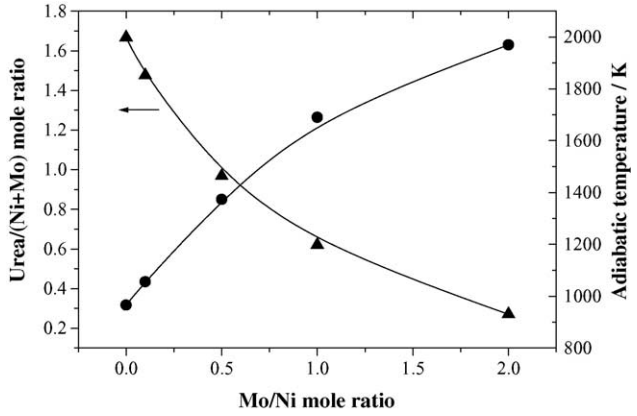

Fig. 3. Influence of the Mo/Ni molar ratio on the adiabatic temperature and the oxidizer–fuel mixture.

Nevertheless, the presence of urea is of paramount importance for combustion synthesis since it increases notably the combustion rate (see Table 1). Urea, even at stoichiometric composition, also undergoes a decomposition process in addition to the combustion process. Hence, when great amount of urea (greater than the optimal redox mixture) is used longer reaction time is required (i.e. 10 min) but also very likely urea contributes to the diminution of the combustion temperature since higher amount of gases are generated upon decomposition–combustion process. This fact could affect the growth and/or formation of hard agglomerates as was determined for the synthesis of Ni-Zn ferrite powders [36].

Fig. 4 compares the laser Raman spectra of urea and different formulations of the Ni-Mo catalyst precursors. The γ-alumina-supported Ni-Mo precursor salts display a major peak at 1012 cm^{-1} and small bands at 1500–1700 and 1178 cm^{-1} assigned to the C–N, C=O bond stretch modes and coupling between the ν_s(CN) and $\rho_s(NH_2)$, respectively, [37,38] of the urea matrix. The Raman peak at 548 cm^{-1} is attributed to the C=O and/or CN deformation vibrations [37]. In addition, a strong peak at 944 and a shoulder at 900 cm^{-1} assigned to the symmetric and asymmetric stretching and a weak band at 353 cm^{-1} attributed to the bending mode of the terminal Mo=O for the Anderson-type heteropolyanion (i.e. $(NH_4)_3[Al(OH)_6Mo_6O_{18}]$) [39] are observed. The deformation of the Mo–O–Mo bridges at 221 cm^{-1} and a weak band at 573 cm^{-1} attributed to the Al–O stretching mode are as well detected [40,41] see (Fig. 4b and c). This entity results from the partial dissolution of alumina and its subsequent complexation with the heptamolybdate anion. A small

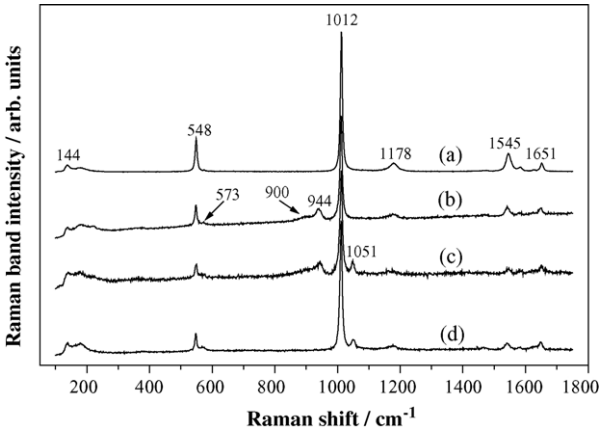

Fig. 4. Laser Raman spectra of the γ-alumina-supported Ni-Mo precursor salts with different formulations and a constant urea/(Ni + Mo) mole ratio of 10. (a) Urea, (b) 12 wt.% MoO_3/γ-Al_2O_3, (c) 3 wt.% NiO-12 wt.% MoO_3/γ-Al_2O_3, (d) 12 wt.% NiO/γ-Al_2O_3.

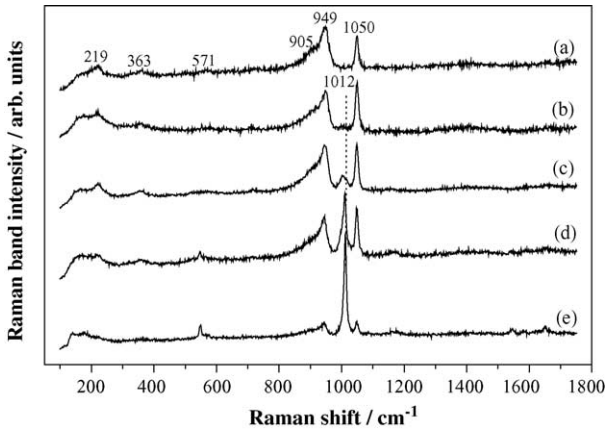

Fig. 5. Laser Raman spectra of the γ-alumina-supported 3Ni-12Mo precursor salts with different urea/(Ni + Mo) mole ratio. (a) 0.0, (b) 0.25, (c) 1.0, (d) 5.0, (e) 10.

Raman peak at 1051 cm^{-1} characteristic of the NO_3^- anion from the promoter precursor salt is illustrated [42,43] whereas Raman peaks characteristic of Ni-oxo species are not clearly observed (Fig. 4d) owing to its weak Raman scatterers.

The influence of the urea on the initial aggregated state of 3Ni-12Mo precursor salts supported on γ-alumina is illustrated in Fig. 5. The spectra of the samples show the main Raman features of 6-molybdoaluminate entities (i.e., Anderson-type heteropolyanion) [39–41], dispersed on alumina (see Fig. 5a). On the other hand, the spectra of the urea-containing catalyst precursors suggest that urea partially hinders the formation of the Anderson-type heteropolyanion. In addition, the main Raman band of the urea matrix at 1012 cm^{-1}, characteristic of the symmetrical C–N stretching vibrational [37], is slightly shifted to lower wavenumbers and becomes broader with urea composition decreasing. This indicates the presence of a weak interaction between urea and the Lewis-type acidic species, probably Ni^{2+} or even cationic species of partially-dissolved alumina.

Several consecutive stages such as melting, dissolution and chemical reactions take place before and upon combustion process to transform the urea and the Ni and Mo precursor salts to well-dispersed oxidic species over alumina surface. A schematic representation of the different states of the catalyst precursors is proposed in Fig. 6. The impregnation or deposition of the precursor salts and urea on alumina at room temperature leads to the formation of poorly-organized 6-molybdoaluminate species as major phase. When the temperature reaches the melting point of urea (i.e. 135 °C), it is spread out over alumina surface and the Ni and Mo salts are partially dissolved and dehydrated, a further increase of the temperature up to 160–175 °C produces a partial decomposition of the precursor salts and of the fuel. It is envisaged that this step facilitates the precipitation of the partially decomposed Ni and Mo precursor salts since the content of urea is significantly reduced. When the sample achieves the ignition temperature (ca. 200 °C) a violent exothermic reaction occurs (simultaneously with the urea thermolysis when a high urea amount is used), releasing heat and different gaseous molecules as a consequence of the total transformation of urea and the precursors to nickel and molybdenum oxides.

The calculated adiabatic temperatures for the synthesis of single and mixed oxides from the nickel nitrate and ammonium heptamolybdate is in the same magnitude order as those determined for synthesis of different single and mixed oxides (i.e. from 700 to 1600 °C) [13,30,31]. The nature of combustion differs from flaming to non-flaming (smouldering) and also from the final product characteristics and its microstructure [13,30]. For the preparation of Al_2O_3-supported oxides this temperature is likely lowered not only by the stoichiometric excess of urea, but also the lower content of the Ni and Mo precursor salts and the combustion-energy dissipation through the support. Taking into account these factors and the low alumina reactivity under combustion condition [15], it is thought that the transformation of the Mo and Ni precursor salts proceeds under a reaction of solid state combustion, hence avoiding the molybdenum oxide loss by sublimation or vaporization. Even though, the UMxC-prepared oxidic precursors was obtained from a combustion process at the ignition temperature of 500 °C instead of a temperature-programmed combustion, one can envisage that in a very short period of time (∼30 s) the sample undergoes water-removal and melting of urea followed by the combustion reaction to produce the oxidic catalyst precursor as was mentioned earlier.

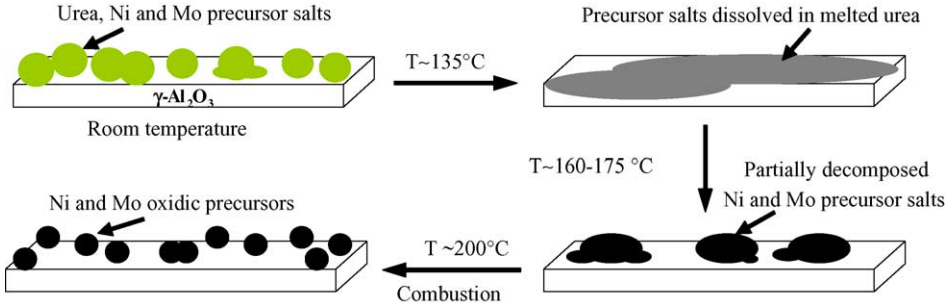

Fig. 6. Schematic representation of the combustion process occurring over the alumina surface upon preparation of Ni-Mo catalyst precursor.

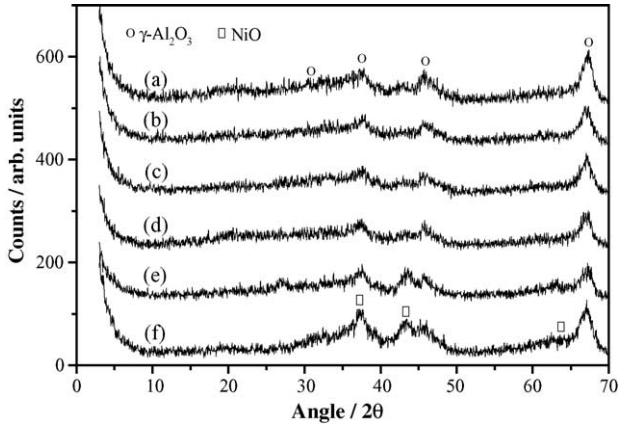

Fig. 7. X-ray diffraction patterns of the γ-Al_2O_3-supported Ni-Mo oxidic precursors prepared by urea–matrix combustion. (a) 12 wt.% MoO_3/γ-Al_2O_3, (b) 1 wt.% NiO-12 wt.% MoO_3/γ-Al_2O_3, (c) 3 wt.% NiO-12 wt.% MoO_3/γ-Al_2O_3, (d) 6 wt.% NiO-12 wt.% MoO_3/γ-Al_2O_3, (e) 12 wt.% NiO-12 wt.% MoO_3/γ-Al_2O_3, (f) 12 wt.% NiO/γ-Al_2O_3.

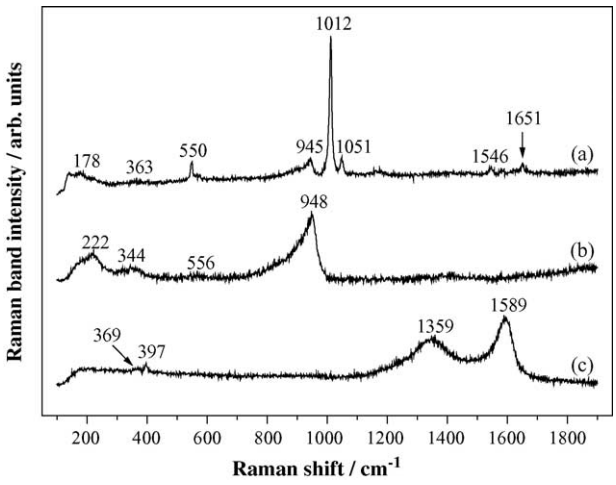

Fig. 8. Laser Raman spectra of 3 wt.% NiO-12 wt.% MoO_3/γ-Al_2O_3 catalyst under different stages of preparation. (a) Dried in high vacuum at room temperature, (b) combusted at 500 °C for 10 min, (c) sulfurized at 500 °C using thiophene as sulfurizing agent.

3.2. Characterization and HDS performance of the γ-Al_2O_3-supported Ni-Mo catalysts

3.2.1. X-ray diffraction and laser Raman spectroscopy

The powder X-ray diffraction patterns of the monometallic (Ni or Mo) and bimetallic (Ni and Mo) catalyst oxidic precursors are shown in Fig. 7. The XRD pattern of 12 wt.% MoO_3/γ-Al_2O_3 shows the main diffraction peaks of γ-Al_2O_3 support (PDF No. 48-367), taken from the PDF-ICDD database crystalline materials [44]. Typical features of molybdenum oxides are not observed owing to a high dispersion on alumina and/or poor crystalline structure, Fig. 7a. On the other hand, the bimetallic oxidic precursors with variable nickel loading display no defined additional XRD peaks up to 6.0 wt.% however for greater nickel loading (i.e., 12 wt.%) a new broad peak at ∼37 and 43.3° in 2θ characteristic of NiO (PDF No. 55-1159) are clearly observed (see Fig. 7e and f). These findings indicate that nickel loadings lower than 6.0 wt.% lead to the formation of highly dispersed and/or poorly-ordered Ni-oxo species on alumina surface whereas higher promoter loadings cause the formation and segregation of NiO. The XRD patterns of the sulfurized samples (not shown) suggest the formation of poorly crystalline and/or highly dispersed Mo and Ni sulfide on γ-alumina since their XRD peaks were not observed.

Fig. 8 compares the effect of the different stages (i.e., drying, combustion and sulfurization) on a typical sample. Again the dried sample displayed the major peaks characteristic of urea matrix [37,38] (Fig. 8a). The Raman bands

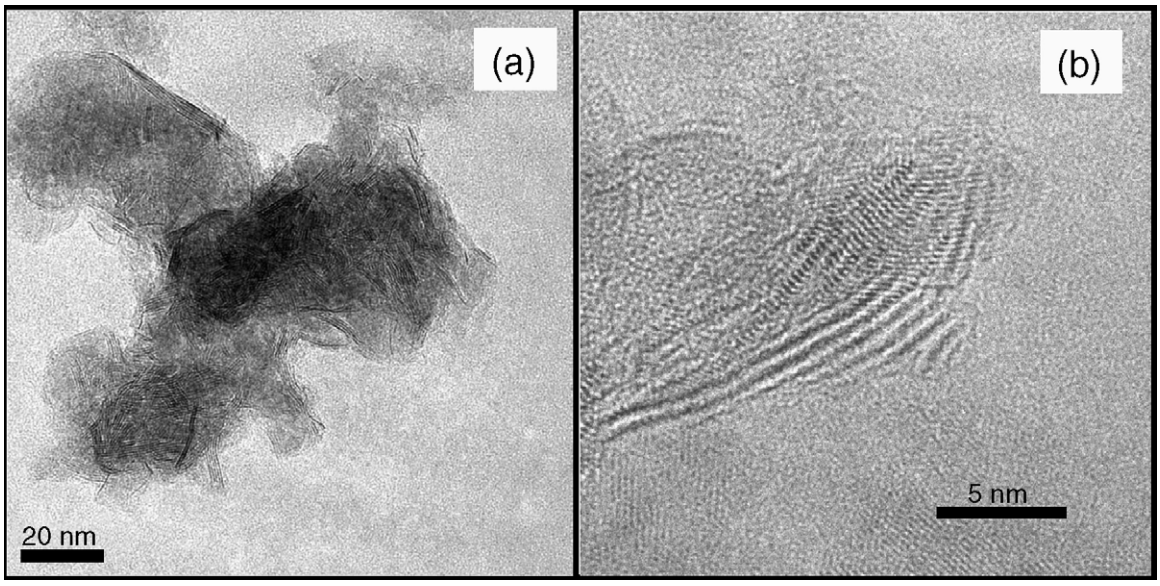

Fig. 9. HRTEM images of the Ni-MoS_2/γ-Al_2O_3 HDS catalysts prepared by urea–matrix combustion method.

associated with the Mo-oxo species are also observed. After combustion, the spectrum displayed a dominant asymmetric feature at 948 cm^{-1} and a small band at 344 cm^{-1}, attributed to the symmetric and bending mode of the terminal Mo=O bond of octahedrally coordinated Mo species for hydrated $Mo_7O_{24}^{6-}$ anion, respectively (Fig. 8b). In addition, the Raman bands at ~556 and 222 cm^{-1} are associated with the symmetric and deformation modes of the Mo–O–Mo bridge for the polymolybdate species [45–49], respectively. The characteristic Raman features of NiO were not observed, likely due to the incorporation of the promoter into the structure of the Mo-oxo anion. In fact, it has been claimed that isopolymolybdate of nickel [50] and Ni heteropolymolybdates [51] might lead to the formation of the HDS active phase. The Raman peaks of urea and residual carbon were not detected either, indicating a total extension of the combustion reaction in line with the TGA results.

On the other hand, the Raman spectrum of the sulfurized catalyst reveals two major Raman features: a strong peak at 1589 and a broad band around 1359 cm^{-1} characteristic of carbon material deposited during sulfurizing process when thiophene is employed as sulfurizing agent (Fig. 8c). The former is associated with the G peak of graphitic carbon (E_{2g} symmetry) and the latter is attributed to A_{1g} disorder mode (D peak) because of the small crystallite size of graphite [52–54]. In addition, this spectrum shows two weak peaks at 369 and 397 cm^{-1} attributed to strongly distorted-MoS_2 along the basal plane since the Mo–S stretching mode (E^1_{2g}) along the basal plane and the S–Mo–S bond mode along the *c*-axis (A_{1g}) is observed at 381 and 405 cm^{-1} for a well-ordered MoS_2 structure [12]. From these findings one can conclude that poorly-ordered Mo-oxo entities over alumina surface form polymolybdate species after the combustion process. These species lead to the formation of strongly distorted-MoS_2 and graphitic carbon when thiophene is used as sulfurizing agent.

Representative HRTEM images in different nano-scale of 3Ni-12MoS_2/γ-Al_2O_3 catalyst are shown in Fig. 9. The micrographs display mainly the edge or prism planes oriented along or roughly parallel to the electron beam direction [55,56] with layer stacking spacing of ca. 6 Å characteristic of bulky MoS_2 [57]. However, other orientations such as the basal planes and the (1 1 0) orientation were also observed but in less extent [58]. In addition, dislocations where the slabs are partially intercalated by another slab and bent on a longer scale to maximize the interaction with the surface are also observed, see image Fig. 9b. On the other hand, the degree of

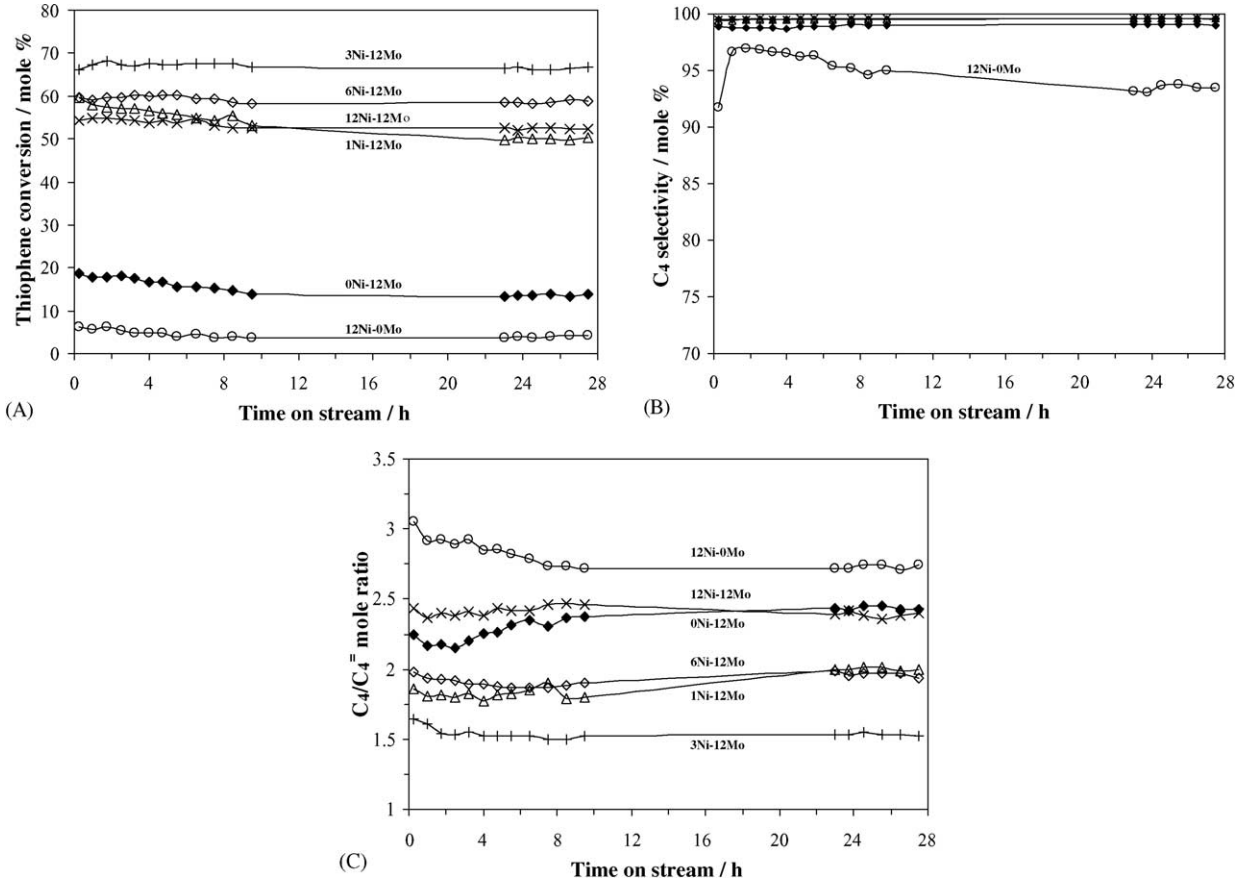

Fig. 10. (A) Catalytic behaviour and (B) and (C) product distribution vs. time on stream of γ-Al_2O_3-supported Ni-Mo HDS catalysts at 350 °C, p = 0.1 MPa and υ = 100 mL (g_{cat} min)$^{-1}$.

stacking is around 3–4 layer and the slab length distribution are fairly broad with an average slab length of ca. 3 nm, owing to the relatively high sulfurizing temperature (i.e., 450 °C). The images are quite similar to the Co-promoted MoS_2/γ-Al_2O_3 HDS catalysts using thiophene as sulfurizing agent as well [12].

3.3. HDS catalytic performance

The time-dependence of thiophene conversion for γ-Al_2O_3-supported Ni-Mo HDS catalysts with variable Ni and fixed Mo compositions is shown in Fig. 10A. The Ni-promoted Mo catalysts showed thiophene conversions four to five times greater than those for the unpromoted Mo catalyst. Furthermore, the Ni-Mo HDS catalysts illustrated practically invariable HDS activity with the time on stream. Except for 1Ni-12Mo catalyst, which underwent a slight decrease of the thiophene conversion similar to the monometallic (Ni or Mo) catalysts, achieving the steady state after 10 h of reaction. On the other hand, the C_4 product distribution obtained through the removal of sulphur from thiophene (C_4H_4S) was not significantly affected by neither the time on stream nor the presence of nickel since C_4 is the major product for Mo-containing catalysts (i.e. greater than 99%) [8]. Also, Ni monometallic catalyst showed C_4 selectivity greater than 90% and the remaining part was of lighter hydrocarbons (C_1–C_3 compounds) (Fig. 10B). These findings indicate that the promoter effect is closely linked to HDS activity rather than the selectivity to C_4 compounds. The $C_4/C_4^=$ mole ratio again did not change significantly with the time on stream however this was clearly affected by the nickel composition, Fig. 10C.

Fig. 11 illustrates the influence of the relative Ni molar composition on the synergistic effect (SE) and the $C_4/C_4^=$ mole ratio. Since butane is a molecule generated by hydrogenation (HYD) of C_4-unsaturated compounds produced through the hydrogenolysis of thiophene and/or β-H elimination of intermediate thiophene compounds (HDS) [59], the $C_4/C_4^=$ mole ratio can be a convenient indicator of the relative rate of HYD to HDS reactions. It was observed a strong increase of the SE at low nickel composition achieving a maximum in Ni/(Ni + Mo) mole ratio of 0.33 and then decrease at higher content. An opposite trend but less pronounced was noted for the $C_4/C_4^=$ mole ratio. Indeed, at approximately iso-conversion (i.e., 50%), the relative rate of HYD to HDS for Ni/(Ni + Mo) of 0.14 increases just by 20% compared with the Ni mole fraction of 0.66, indicating that a slight antagonism effect on the $C_4/C_4^=$ mole ratio is present. Therefore, synergistic effect increases markedly the C–S bond cleavage reaction but to a much lesser extent affects the relative rate of hydrogen transfer reactions.

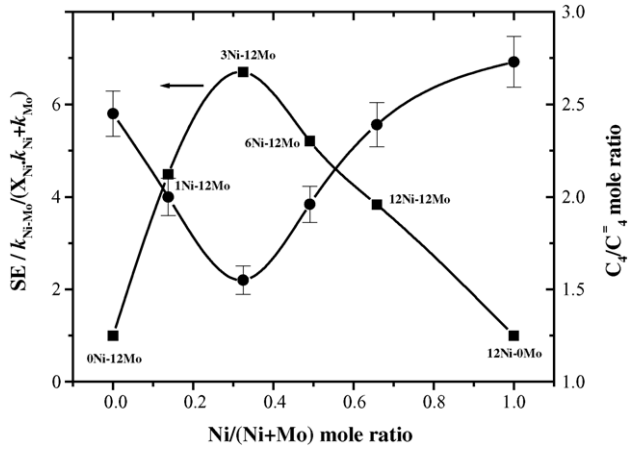

Fig. 11. Dependence of the synergistic effect (SE) and the $C_4/C_4^=$ mole ratio on the Ni-Mo catalyst composition.

The optimal composition and the qualitative behaviour of the promoter effect of nickel on Mo-based HDS catalyst are rather similar to the earlier reports of Al_2O_3-supported Ni-Mo catalysts [60,61]. However, the optimal promoter effect (i.e., k_{Ni-Mo}/k_{Mo}) of the combustion-prepared catalyst was slightly lower (ca. 15%) than that recently given by Zdražil over impregnation-prepared Ni-Mo catalyst [62]. This is probably due to the coverage of the most active HDS sites by deposition of graphitic carbon upon sulfurizing process when thiophene is employed as a sulfurizing agent and/or the lateral growing of MoS_2 by sintering.

An HDS apparent activation energy (E_a^{app}) derived from Arrehenius plot of 59 ± 8 kJ/mol for the catalyst with optimal composition (i.e., 3Ni-12Mo) was obtained. This is in rather good agreement with the figure reported by Borgna et al. [63,64] and Ledoux et al. [65]. This suggests that carbon deposited from the sulfurizing process does not significantly inhibit the hydrodesulfurization reaction, probably due to its participation in the formation of the HDS active sites, as has been previously reported [12,66,67]. Therefore, the main cause of the slightly lower promoter effect is due to the lateral growing of MoS_2 rather than the deposition of carbon. At higher temperatures of 583 K, on the other hand, the apparent activation energy decreases to 37 kJ/mol. This behaviour is not ascribed to mass-transfer limitations since experiments with different catalysts particles sizes revealed that these limitations are absent. This result has been attributed to the changes in the rate limiting step in the HDS reaction mechanism [68] and/or to a decrease of reactant surface coverage as temperature increases [64,69].

It must be pointed out that the γ-alumina-supported 3Ni-12Mo HDS catalysts prepared using different urea/(Ni + Mo) mole ratio and also combusted at different ignition temperatures (i.e. 300–600 °C) for 10 min showed similar catalytic behaviour (i.e., HDS activity and product distribution) than that presented in Fig. 11. This indicates that both parameters do not affect significantly the catalytic properties of 3Ni-12Mo HDS catalyst, probably due to a stabilizing effect of the alumina upon the combustion process and/or to the carbon material deposited during sulfurization process. Indeed, Chianelli and co-workers have found that the interaction between the carbon and the edge planes of MoS_2 not only favours the

formation of surface "carbonsulfide" phase, but also stabilizes texturally the sulfide particles [66,67], which would be reflected in a remarkable catalytic stability.

4. Concluding remarks

A new approach named urea–matrix combustion method based on combustion and decomposition processes has been successfully applied for the first time to prepare alumina-supported Ni-Mo oxidic precursor. Several consecutive stages such as melting, dissolution and chemical reactions take place before and during combustion process. The deposition of the precursor salts and urea as fuel on alumina at room temperature leads to the formation of poorly-crystallized Mo-oxo species as the major phases. After the combustion process well-dispersed Ni (at compositions not greater than 6 wt.%) and polymolybdate species on alumina surface are formed. There is not evidence of residual carbon after combustion process. The sulfurization process using thiophene in H_2 as sulfurizing agent facilitates the formation of graphitic carbon and a strongly distorted-MoS_2 type structure.

The urea–matrix combustion method is a simple method and the catalysts can be prepared in a short period of thermal treatment. Urea employed as fuel not only increases the combustion rate, but also undergoes a decomposition process (endothermic reaction) that could contribute to the reduction of the combustion temperature. This method gives highly active γ-Al_2O_3-supported Ni-Mo HDS catalyst, which shows a comparable promoter effect to that of impregnation-prepared catalyst. In addition, an opposite relation between the activity and the hydrogenation properties was observed indicating that highly active HDS catalyst requires low consumption of hydrogen. Finally, both the ignition temperature and the urea-oxidizer ratio produce no significant changes in the HDS catalytic properties of Ni-Mo-based catalysts.

Acknowledgement

S.L. González-Cortés is indebted to the ULA and FONACIT (Venezuela) for financial support.

References

[1] EP directive 2003/17/EC, Official J. Eur. Union L76, 46 (2003) 10.
[2] I.V. Babich, J.A. Moulijn, Fuel 82 (2003) 607.
[3] R. Prins, H.J. de Beer, G.A. Somorjai, Catal. Rev.-Sci. Eng. 31 (1989) 1.
[4] R.R. Chianelli, Catal. Rev.-Sci. Eng. 25 (1984) 361.
[5] H. Topsøe, B. Clausen, Catal. Rev.-Sci. Eng. 26 (1984) 420.
[6] P.T. Vasudevan, J.L.G. Fierro, Catal. Rev.-Sci. Eng. 38 (1996) 161.
[7] R. Prins, Adv. Catal. 46 (2001) 399.
[8] H. Topsøe, B.S. Clausen, F.E. Massoth, in: J.R. Anderson, M. Boudart (Eds.), Hydrotreating Catalysis, Science and Technology, Springer-Verlag, Berlin, 1996.
[9] L. Qu, W. Zhang, P.J. Kooyman, R. Prins, J. Catal. 215 (2003) 7.
[10] A. Calafat, J. Laine, A. López-Agudo, J.M. Palacios, J. Catal. 162 (1996) 20.
[11] J.L. Brito, J. Laine, J. Catal. 139 (1993) 540.
[12] S.L. González-Cortés, T-C. Xiao, P.M.F.J. Costa, B. Fontal, M.L.H. Green, Appl. Catal. A: Gen. 270 (2004) 209.
[13] K.C. Patil, S.T. Aruna, T. Mimani, Curr. Opin. Solid State Mater. Sci. 6 (2002) 507.
[14] G. Xanthopoulou, G. Vekinis, Appl. Catal. B: Environ. 19 (1998) 37.
[15] J.J. Moore, H.J. Feng, Prog. Mater. Sci. 39 (1995) 275.
[16] J.J. Moore, H.J. Feng, Prog. Mater. Sci. 39 (1995) 243.
[17] G. Xanthopoulou, G. Vekinis, Appl. Catal. A: Gen. 199 (2000) 227.
[18] G. Xanthopoulou, Appl. Catal. A: Gen. 185 (1999) L185.
[19] P. Bera, K.C. Patil, V. Jayaram, G.N. Subbanna, M.S. Hegde, J. Catal. 196 (2000) 293.
[20] P. Bera, K.C. Patil, M.S. Hegde, Phys. Chem. Chem. Phys. 2 (2000) 3715.
[21] M. Adachi, C. Contescu, J.A. Schwarz, J. Catal. 162 (1996) 66.
[22] H. Knözinger, P. Ratnasamy, Catal. Rev.-Sci. Eng. 17 (1978) 31.
[23] R. Murugan, H. Chang, J. Chem. Soc. Dalton Trans. 20 (2001) 3125.
[24] I.B. Sharma, S. Batra, J. Therm. Anal. 41 (1994) 1075.
[25] D.R. Lide (Ed.), CRC Handbook of Chemistry and Physics, 84th ed., CRC press, Boca Raton, 2003.
[26] M.A.A. Elmasry, A. Gaber, E.M.H. Khater, J. Thermal. Anal. 52 (1998) 489.
[27] J.B. Peri, J. Phys. Chem. 69 (1965) 211.
[28] J.H. de Boer, J.M.H. Fortuin, B.C. Lippens, W.H. Meijs, J. Catal. 2 (1963) 1.
[29] S.R. Jain, K.C. Adiga, V.R. Pai Verneker, Combust. Flame 40 (1981) 71.
[30] K. Suresh, K.C. Patil, in: K.J. Rao (Ed.), Perspective in Solid State Chemistry, Narosa Publishing House, New Delhi, 1995, p. 376.
[31] D.A. Fumo, M.R. Morelli, A.M. Segadães, Mater. Res. Bull. 31 (1996) 1243.
[32] J.B. Holt, Z.A. Munir, J. Mater. Sci. 21 (1986) 251.
[33] J.A. Dean (Ed.), Lange's Handbook of Chemistry, 12th ed., McGraw-Hill, New York, 1979.
[34] M.T. Colomer, D.A. Fumo, J.R. Jurado, A.M. Segadâes, J. Mater. Chem. 9 (1999) 2505.
[35] M. Morishita, A. Navrotsky, J. Am. Ceram. Soc. 86 (2003) 1937.
[36] A.C.F.M. Costa, M.R. Morelli, R.H.G.A. Kiminami, J. Mater. Synth. Process. 9 (2001) 347.
[37] R. Keuleers, H.O. Desseyn, B. Rousseau, C. Van Alsenoy, J. Phys. Chem. A. 103 (1999) 4621.
[38] B. Rousseau, C. Van Alsenoy, R. Keuleers, H.O. Desseyn, J. Phys. Chem. A. 102 (1998) 6540.
[39] X. Carrier, J.F. Lambert, M. Che, J. Am. Chem. Soc. 119 (1997) 10137.
[40] L. Le Bihan, P. Blanchard, M. Fournier, J. Grimblot, E. Payen, J. Chem. Soc., Faraday Trans. 94 (1998) 937.
[41] X. Carrier, J.F. Lambert, S. Kuba, H. Knözinger, M. Che, J. Mol. Struct. 656 (2003) 231.
[42] V. Vendange, D.J. Jones, Ph. Colomban, J. Phys. Chem. Solids 57 (1996) 1907.
[43] M.R. Waterland, D. Stockwell, A.M. Kelley, J. Chem. Phys. 114 (2001) 6249.
[44] JCPDS Powder Diffraction File, Int. Centre for Diffraction Data, Swarthmore, PA, 1989.
[45] G. Mestl, T.K.K. Srinivasan, Catal. Rev.-Sci. Eng. 40 (1998) 451.
[46] F.D. Hardcastle, I.E. Wachs, J. Raman Spectrosc. 21 (1990) 683.
[47] D.S. Kim, K. Segawa, T. Soeya, I.E. Wachs, J. Catal. 136 (1992) 539.
[48] H. Hu, I.E. Wachs, J. Phys. Chem. 99 (1995) 10911.
[49] G. Mestl, J. Mol. Catal. A: Chem. 158 (2000) 45.

[50] S. Kasztelan, J. Grimblot, J.P. Bonnelle, J. Phys. Chem. 91 (1987) 1503.
[51] H. Jeziorowski, H. Knoezinger, Appl. Surf. Sci. 5 (1980) 335.
[52] F. Tuinstra, J.L. Koenig, J. Chem. Phys. 53 (1970) 1126.
[53] D.S. Knight, W.B. White, J. Mater. Res. 4 (1989) 385.
[54] A. Ermolieff, A. Chabli, F. Pierre, G. Rolland, D. Rouchon, C. Vannuffel, C. Vergnaud, J. Baylet, M.N. Séméria, Surf. Interface Anal. 31 (2001) 185.
[55] F. Delannay, Appl. Catal. 16 (1985) 135.
[56] K.C. Pratt, J.V. Sanders, V. Christov, J. Catal. 124 (1990) 416.
[57] T.F. Hayden, J.A. Dumesic, J. Catal. 103 (1987) 366.
[58] R.M. Stockmann, H.W. Zandbergen, A.D. van Langeveld, J.A. Moulijn, J. Mol. Catal. A: Chem. 102 (1995) 147.
[59] R. Prins, in: G. Ertl, H. Knozinger, J. Weitkamp (Eds.), Handbook of Heterogeneous Catalysis, vol. 4, Wiley-VCH, Weinheim, 1997, p. 1908.
[60] S.P. Ahuja, M.L. Derrien, J.F. Le Page, Ind. Eng. Chem. Prod. Res. Dev. 9 (1970) 272.
[61] V.H.J. de Beer, T.H.M. van Sin Fiet, J.F. Engelen, A.C. van Haandel, M.W.J. Wolfs, C.H. Amberg, G.C.A. Schuit, J. Catal. 27 (1972) 357.
[62] M. Zdražil, Catal. Today 86 (2003) 151.
[63] A. Borgna, E.J.M. Hensen, L. Coulier, M.H.J.M. de Croon, J.C. Schouten, J.A.R. van Veen, J.W. Niemantsverdriet, Catal. Lett. 90 (2003) 117.
[64] A. Borgna, E.J.M. Hensen, J.A.R. van Veen, J.W. Niemantsverdriet, J. Catal. 221 (2004) 541.
[65] M.J. Ledoux, O. Michaux, G. Agostine, J. Catal. 102 (1986) 275.
[66] G. Berhault, L. Cota Araiza, A. Duarte Moller, A. Mehta, R.R. Chianelli, Catal. Lett. 78 (2002) 81.
[67] G. Berhault, A. Mehta, A.C. Pavel, J. Yang, L. Rendon, M.J. Yacaman, L. Cota Araiza, A. Duarte Moller, R.R. Chianelli, J. Catal. 198 (2001) 9.
[68] A.N. Startsev, Catal. Rev.-Sci. Eng. 37 (1995) 353.
[69] E.J.M. Hensen, M.J. Vissenberg, V.H.J. de Beer, J.A.R. van Veen, R.A. van Santen, J. Catal. 163 (1996) 429.